

000 001 002 003 004 005 ACTION-AWARE DYNAMIC PRUNING FOR EFFICIENT 006 VISION-LANGUAGE-ACTION MANIPULATION 007 008 009

010 **Anonymous authors**
011 Paper under double-blind review
012
013
014
015
016
017
018
019
020
021
022
023
024
025
026
027
028

ABSTRACT

029
030
031
032
033 Robotic manipulation with Vision-Language-Action models requires efficient in-
034 ference over long-horizon multi-modal context, where attention to dense visual
035 tokens dominates computational cost. Existing methods optimize inference speed
036 by reducing visual redundancy within VLA models, but they overlook the varying
037 redundancy across robotic manipulation stages. We observe that the visual token
038 redundancy is higher in coarse manipulation phase than in fine-grained operations,
039 and is strongly correlated with the action dynamic. Motivated by this observation,
040 we propose Action-aware **Dynamic Pruning (ADP)**, a multi-modal pruning frame-
041 work that integrates text-driven token selection with action-aware trajectory gating.
042 Our method introduces a gating mechanism that conditions the pruning signal on
043 recent action trajectories, using past motion windows to adaptively adjust token
044 retention ratios in accordance with dynamics, thereby balancing computational
045 efficiency and perceptual precision across different manipulation stages. Extensive
046 experiments on the LIBERO suites and diverse real-world scenarios demonstrate
047 that our method significantly reduces FLOPs and action inference latency (*e.g.*
048 1.35 \times speed up on OpenVLA-OFT) while maintaining competitive success rates
049 (*e.g.* 25.8% improvements with OpenVLA) compared to baselines, thereby provid-
050 ing a simple plug-in path to efficient robot policies that advances the efficiency and
051 performance frontier of robotic manipulation.
052
053

1 INTRODUCTION

034 Large vision language models Liu et al. (2023c;b; 2024a); Team et al. (2023); Awadalla et al. (2023)
035 have recently been extended into Vision–Language–Action (VLA) models Kim et al. (2024; 2025);
036 Black et al. (2024); Li et al. (2024); Brohan et al. (2024); Wen et al. (2025b;a); Bjorck et al. (2025)
037 that map both the visual observation and language instruction to executable robot actions. In the
038 mainstream pipeline, a vision encoder produces dense visual tokens from one or more camera views,
039 a projector aligns them to the language space, and an LLM fuses all modalities to predict actions.
040 However, this multi-modal design introduces long input sequences with numerous visual tokens that
041 are only weakly relevant to the current manipulation operation, which inflates compute, memory
042 footprint, and latency, and it can dilute attention over truly task-relevant cues.
043

044 Existing work pursues efficiency via architectural lightening and modality-aware compression, such as
045 RoboMamba Liu et al. (2024b) that focuses on lightweight designs, DeeR-VLA Yue et al. (2024) that
046 aims at structured pruning/reparameterization, Mole-VLA Zhang et al. (2025) that targets conditional
047 layer activation, VLA-Cache Xu et al. (2025) that focuses on cache reuse, and EfficientVLA Yang
048 et al. (2025) that aims to prune visual tokens via attention. However, a key but underexplored property
049 of robotic manipulation is that **visual redundancy in VLAs is action-aware across different**
050 **manipulation stages**. As Fig. 1 shows, during coarse-grained operations (*e.g.*, relocating), global
051 movement dominates and redundant tokens can be pruned; during fine-grained phases (*e.g.*, grasping),
052 local geometry and detailed cues dominate and preserving full vision is preferred. Moreover, the
053 relevance of visual patches is not only text conditioned (semantics of the instruction) but also *action*
054 *conditioned* (instantaneous end-effector motion and gripper state). Treating all steps uniformly, or
055 ranking tokens solely by mixed attention scores, therefore yields suboptimal pruning schedules that
056 either prune too little (limited savings) or prune too much (accuracy loss), especially in multi-view
057 settings (scene and wrist/gripper cameras) where importance is unevenly distributed across time.

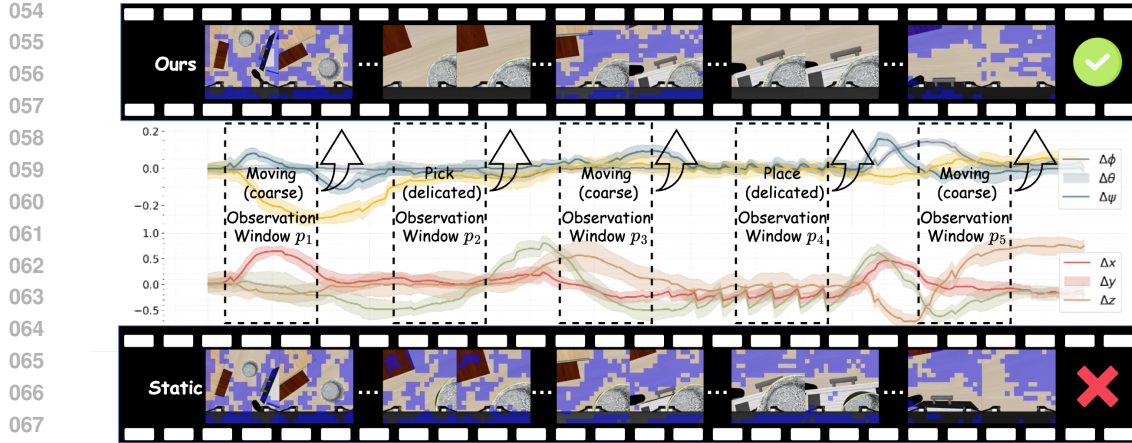


Figure 1: **Action-aware dynamic pruning vs. static pruning.** We visualize five *past* observation windows as cases from a manipulation episode that condition the *current anticipatory* window. p_1 , p_3 and p_5 reflect coarse phases, prompting the gate to *enable* pruning to suppress redundant tokens, whereas p_2 and p_4 are delicate phases requiring detail vision context, so pruning is *disabled* and full vision is used. The curves depict robot’s motion that drives the gating rule.

To address this challenge, we introduce Action-aware Dynamic Pruning (ADP), a plug-and-play strategy that reduces computation while preserving manipulation fidelity. ADP is built on two complementary ideas: (1) *Text-driven Pruning* evaluates the relevance of visual patch using cross-modal similarities, selecting only the most relevant tokens before entering deep fusion in the subsequent layers. (2) *Action-aware Dynamics* modulate whether pruning is activated at a given step using a lightweight decision signal derived from the end-effector trajectory within each action window. Specifically, when the recent motion magnitude is relatively low compared to past motion statistics (delicate phases), pruning is disabled to preserve the full visual field for precise control. Conversely, when the motion magnitude is relatively high compared to past motion statistics (coarse phases), pruning is engaged to suppress redundancy and save FLOPs. We implement a gated mechanism that treats recent action statistics as a pruning signal over sliding trajectory windows, adaptively adjusting retention ratios according to motion dynamics and balancing efficiency with precision across manipulation stages. Our contributions can be summarized as: (1) We show that the importance of the visual token in VLA models varies within different stages of robotic manipulation. This insight motivates our dynamic pruning method tailored to manipulation phases compared to static pruning approaches. (2) We propose *text-driven action-aware pruning* that combines task instruction relevance with a gating rule based on end-effector motion, enabling adaptive switching between pruned and full-vision states. (3) We present a principled complexity analysis and extensive experiments in simulation and real-world settings, demonstrating that our method reduces FLOPs and latency while maintaining fine visual details required for successful manipulation.

2 PRELIMINARY

The mainstream vision–language–action paradigm extends large vision–language models to generate executable robot actions from multi-modal inputs—visual observations (scene and wrist/gripper views) and task instructions. A pre-trained vision encoder produces visual tokens, a projector aligns them to the LLM token space, and the LLM fuses modalities and autoregressively emits action tokens, which are de-tokenized into a continuous 7-dimensional robot action.

Formally, given a sample of a scene image $I^s \in \mathbb{R}^{H \times W \times 3}$, a gripper view $I^g \in \mathbb{R}^{H \times W \times 3}$, and a task instruction $I^t \in \mathbb{R}^{N \times L}$, the vision encoder f_{enc}^v (DINOv2 Oquab et al. (2023) and SigLIP Zhai et al. (2023)) and text tokenizer f_{enc}^t project the multi-modal data into the same latent dimension space:

$$\mathbf{X}^{\text{vis}} = f_{\text{enc}}^v(I^s, I^g), \quad \mathbf{X}^{\text{txt}} = f_{\text{enc}}^t(I^t), \quad (1)$$

where $\mathbf{X}^{\text{vis}} \in \mathbb{R}^{L_{\text{vis}} \times D}$ and $\mathbf{X}^{\text{txt}} \in \mathbb{R}^{L_{\text{txt}} \times D}$ represent latent embeddings for vision and text.

108 **OpenVLA.** In the latent space, the embedding representations are concatenated into a multi-modal
 109 sequence as:

$$110 \quad \mathbf{X}^m = \mathbf{X}^{[BOS]} \oplus \mathbf{X}^{\text{vis}} \oplus \mathbf{X}^{\text{prop}} \oplus \mathbf{X}^{\text{txt}} \quad (2)$$

111 where \oplus denotes concatenating embeddings of [BOS], vision, text, and proprioceptive (optionally)
 112 along the sequence length dimension, yielding multi-modal inputs $\mathbf{X}^m \in \mathbb{R}^{1+L_{\text{vis}}+L_{\text{txt}}+1}$. The
 113 multi-modal sequence \mathbf{X}^m is then fed into a Large Language Model (LLM) f_{LLM} (Llama2 Touvron
 114 et al. (2023)), which performs contextual reasoning and autoregressively generates an action token
 115 sequence:

$$116 \quad p(\hat{\mathbf{a}} \mid \mathbf{X}^m) = \prod_{j=1}^7 f_{\text{LLM}}(\hat{a}_j \mid \mathbf{X}^m, \hat{a}_{<j}), \quad (3)$$

119 where $\hat{\mathbf{a}} = (\hat{a}_1, \dots, \hat{a}_7) \in \mathbb{T}^7$ and $\mathbb{T} = \{1, \dots, K\}$ denotes the reserved action token space.

120 **OpenVLA-OFT.** For optimize finetuning version, the paradigm shifts to parallel decoding without
 121 traditional autoregressive decoding stage. In the latent space, the method introduces L_{act} placeholder
 122 $\mathbf{X}^{\text{place}}$ as inputs for actions positions:

$$123 \quad \mathbf{X}^m = \mathbf{X}^{[BOS]} \oplus \mathbf{X}^{\text{vis}} \oplus \mathbf{X}^{\text{prop}} \oplus \mathbf{X}^{\text{txt}} \oplus \mathbf{X}^{\text{place}}, \quad (4)$$

124 where $\mathbf{X}^m \in \mathbb{R}^{1+L_{\text{vis}}+L_{\text{txt}}+1+L_{\text{act}}}$ and the first placeholder as current action placeholder and another
 125 $L_{\text{act}} - 1$ actions as future actions. During generation, the LLM directly predicts action tokens at
 126 action chunk in parallel:

$$127 \quad \hat{\mathbf{A}} = f_{\text{LLM}}(\mathbf{X}^m) \big|_{\text{place}} \in \mathbb{T}^{L_{\text{act}} \times 7}, \quad (5)$$

128 where $\hat{\mathbf{A}} = [\hat{\mathbf{a}}_1; \dots; \hat{\mathbf{a}}_{L_{\text{act}}}]$, and each $\hat{\mathbf{a}}_i = (\hat{a}_{i,1}, \dots, \hat{a}_{i,7}) \in \mathbb{T}^7$ represents the tokenized 7-DoF
 129 action predicted at the i -th placeholder position. To expand action representation ability, the oft
 130 version also introduce the continuous control with token-level modeling, which each dimension of
 131 the continuous action is uniformly discretized into 256 bins. During generation, the 7 degrees of
 132 freedom action follows the standard gripper parameterization:

$$134 \quad \hat{\mathbf{a}}^c = [\Delta x, \Delta y, \Delta z, \Delta \phi, \Delta \theta, \Delta \psi, g]^\top, \quad (6)$$

135 where $(\Delta x, \Delta y, \Delta z)$ denote Cartesian displacements, $(\Delta \phi, \Delta \theta, \Delta \psi)$ denote Euler-angle rotations
 136 (roll, pitch, yaw), and g denotes the gripper.

138 3 RELATED WORK

140 **Vision-Language-Actions.** Vision-Language-Action (VLA) models extend large vision-language
 141 models with an action generator that links multimodal perception to low-level robot control. They take
 142 images and text instructions, encode them into a shared latent space, then decode it into executable
 143 actions. Early approaches Chi et al. (2023); Kim et al. (2024) map multimodal embeddings to
 144 discrete tokens, while more recent works Wen et al. (2025b); Kim et al. (2025) emphasize continuous
 145 parallel decoding actions for improving performance. To this end, lightweight MLPs, diffusion-based
 146 decoders, and parallel decoding strategies have been introduced to transform hidden states into
 147 temporally consistent trajectories. Representative architecture include CogACT Li et al. (2024),
 148 OpenVLA Kim et al. (2024), OpenVLA-OFT Kim et al. (2025), and π series Black et al. (2024),
 149 which adopt diffusion modules for iterative refinement of continuous actions, as well as optimized
 150 fine-tuning frameworks that leverage placeholder tokens for parallel action prediction.

151 **Efficient Robotic Manipulations.** The high computational complexity of Vision-Language-Action
 152 (VLA) models poses significant efficiency challenges for real-time robotic control. To address this,
 153 recent works have proposed efficiency-oriented strategies that can be broadly divided into training-
 154 aware and training-free approaches. Training-aware methods, such as RoboMamba Liu et al. (2024b)
 155 and DeeR-VLA Yue et al. (2024), redesign architectures or apply compression and pruning during
 156 training, achieving notable speedups while preserving accuracy. For instance, DeeR-VLA Yue et al.
 157 (2024) introduces dynamic reparameterization and structured pruning to reduce FLOPs, and Mole-
 158 VLA Zhang et al. (2025) selectively activates subsets of model layers conditioned on task demands,
 159 yielding scalable deployment. On the other hand, training-free methods aim to accelerate inference
 160 without retraining. VLA-Cache Xu et al. (2025) reuses keys and values of uninformative tokens
 161 between consecutive steps to save computation, while EfficientVLA Yang et al. (2025) retain task-
 162 relevant patches identified via attention maps. However, these methods typically rely on single-layer
 163 heuristics or static rules that may overlook stage-dependent redundancy in manipulation tasks.

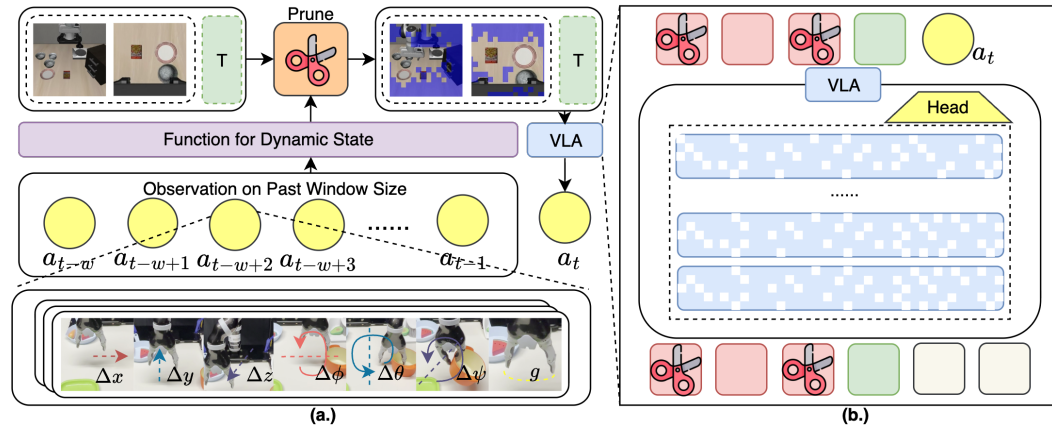


Figure 2: Overview of our proposed **Action-aware Dynamic Pruning (ADP)** for Vision-Language-Action models. **(a.)** Action-aware gating: the pruning function adaptively determines whether to prune based on recent end-effector trajectories ($\Delta x, \Delta y, \Delta z, \Delta \phi, \Delta \theta, \Delta \psi, g$), enabling dynamic pruning. **(b.)** Anticipatory pruning: task-relevant visual tokens are selected via attention-based relevance, while redundant patches are discarded before entering the VLA backbone.

4 METHODOLOGY

In this section, we introduce our proposed method Action-aware Dynamic Pruning (ADP) in VLAs for robotic manipulations. We first introduce text-driven pruning that identifies text-relevant tokens in Section 4.1 and then introduce action-aware dynamics that dynamically modulates the pruning strategy according to the past observed actions in Section 4.2.

4.1 TEXT-DRIVEN ANTICIPATORY PRUNING

Before entering the LLM, the multimodal sequence \mathbf{X} still contains a large number of redundant visual tokens, which increase computation and dilute attention focus. To mitigate this redundancy, we compute the relevance of visual tokens with respect to task instructions at each layer, which is shown in Figure 3. Let the hidden state at layer l be $\mathbf{H}^{(l)} \in \mathbb{R}^{S \times D}$ ($\mathbf{H}^{(0)} = \mathbf{X}^m$ in Eq. 2). We partition $\mathbf{H}^{(l)}$ into the vision and text subsets $\mathbf{H}_{\text{vis}}^{(l)} \in \mathbb{R}^{L^{\text{vis}} \times D}$ and $\mathbf{H}_{\text{txt}}^{(l)} \in \mathbb{R}^{L^{\text{txt}} \times D}$. Applying the projection matrices, we obtain query and key representations:

$$\mathbf{Q}^{(l)} = \mathbf{H}_{\text{txt}}^{(l)} W_Q^{(l)}, \quad \mathbf{K}^{(l)} = \mathbf{H}_{\text{vis}}^{(l)} W_K^{(l)}, \quad (7)$$

reshaped into multi-head form $\mathbf{Q}^{(l)} \in \mathbb{R}^{N^h \times L^{\text{txt}} \times d}$ and $\mathbf{K}^{(l)} \in \mathbb{R}^{N^h \times L^{\text{vis}} \times d}$. The scaled dot-product similarity is then computed as

$$\mathbf{A}^{(l)} = \frac{\mathbf{Q}^{(l)} (\mathbf{K}^{(l)})^\top}{\sqrt{d}} \in \mathbb{R}^{N^h \times L^{\text{txt}} \times L^{\text{vis}}}, \quad (8)$$

where each entry measures the degree to which a text token attends to a visual patch. To derive a global importance score per visual token, we average across heads and text queries:

$$\Phi^{(l)}(v) = \frac{1}{N^h \cdot L_{\text{txt}}} \sum_{h=1}^{N^h} \sum_{t=1}^{L_{\text{txt}}} \mathbf{A}_{h,t,v}^{(l)}, \quad (9)$$

$$\mathbf{X}_{\text{keep}} = \text{Top-K}(\Phi^{(l)}, k), \quad k = \lfloor \rho \cdot L^{\text{vis}} \rfloor, \quad (10)$$

where $v \in \{1, \dots, L^{\text{vis}}\}$ indexes visual tokens, N^h is the number of attention heads, L^{txt} is the text sequence length, and L^{vis} is the total number of visual tokens. In multi-view scenarios with C input images (e.g., scene and wrist views), each contributing L_c^{vis} patches such that $\sum_{c=1}^C L_c^{\text{vis}} = L^{\text{vis}}$, the retention quota is distributed across views by a weighting vector $\alpha \in \mathbb{R}^C$ with $\sum_{c=1}^C \alpha_c = 1$. The remain visual tokens kept for view c is

$$\mathbf{X}_{(c)}^{\text{vis}} = \text{Top-K}(\Phi_{(c)}^{(l)}, k_c), \quad k_c = \lfloor \alpha_c \cdot k \rfloor, \quad (11)$$

216 where $\Phi_{(c)}^{(l)}$ denotes the importance scores restricted
 217 to view c . For each view c , the remain visual tokens
 218 could be represented as:
 219

$$220 \quad \mathbf{X}_{\text{keep}}^{\text{vis}} = \bigcup_{c=1}^C \{ \mathbf{X}_{(c)}^{\text{vis}}[v] \mid v \in \mathbf{X}_{(c)}^{\text{vis}}, \mathbf{X}_{(c)}^{\text{vis}}[v] \in \mathbb{R}^D \}. \quad (12)$$

223 The reduced visual sequence $\mathbf{X}_{\text{keep}}^{\text{vis}}$ is then concatenated
 224 back with other modalities to form the pruned
 225 multimodal sequence:
 226

$$227 \quad \tilde{\mathbf{X}}^m = \mathbf{X}^{\text{[BOS]}} \oplus \mathbf{X}_{\text{keep}}^{\text{vis}} \oplus \mathbf{X}^{\text{prop}} \oplus \mathbf{X}^{\text{txt}} \oplus \mathbf{X}^{\text{act}} \oplus \mathbf{X}^{\text{[EOS]}}, \quad (13)$$

229 where $\tilde{\mathbf{X}}^m$ denotes the dynamically reduced input
 230 propagated to the LLM module.
 231

4.2 ACTION-AWARE DYNAMIC STRATEGY

233 While static pruning can effectively identify task-
 234 relevant visual tokens, not every stage of a manipula-
 235 tion task is suitable for relying solely on the pruned set. In particular, missing fine-grained visual
 236 details may cause failures in operations such as moving, swiping, or aligning objects. The accumula-
 237 tion of such local errors can easily propagate and ultimately cause the entire task to fail. To address
 238 this limitation, we introduce a dynamic visual strategy that adapts the pruning decision to the robot’s
 239 motion state across different task phases, guided by the end-effector (EEF) trajectory within each
 240 action chunk, which focus on capturing both translational displacement and rotational motion.
 241

242 **Windowed trajectory and actions.** Assume i indexes windows and u indexes steps within a
 243 window; b_i and e_i denote the start and end timesteps, and ω matches the OFT action placeholder length.
 244 We treat each decoded action chunk as a temporal window $[b_i, e_i]$ of length $\omega = e_i - b_i + 1$ with actions
 245 $\mathbf{A}_i^c = [\mathbf{a}_{i,1}^c; \dots; \mathbf{a}_{i,\omega}^c] \in \mathbb{R}^{\omega \times 7}$, where $\mathbf{a}_{i,u}^c = [\Delta x_{i,u}, \Delta y_{i,u}, \Delta z_{i,u}, \Delta \phi_{i,u}, \Delta \theta_{i,u}, \Delta \psi_{i,u}, g_{i,u}]^\top$
 collects per-step translational and rotational increments and the gripper command.
 246

247 **Definition 4.1** (Windowed FK for EEF Position). *Let $T_t \in SE(3)$ be the EEF pose at time t , and
 248 $\pi : SE(3) \rightarrow \mathbb{R}^3$ extract its translation. With body-frame (right-multiply) composition,*

$$249 \quad \mathbf{p}_{b_i+u} \triangleq \pi \left(T_{b_i} \prod_{k=1}^u \begin{bmatrix} R_{i,k} & \mathbf{v}_{i,k} \\ \mathbf{0}^\top & 1 \end{bmatrix} \right), \quad T_{b_i+u} \triangleq T_{b_i+u-1} \begin{bmatrix} R_{i,u} & \mathbf{v}_{i,u} \\ \mathbf{0}^\top & 1 \end{bmatrix}, \quad (14)$$

252 where $\mathbf{v}_{i,u} = [\Delta x_{i,u}, \Delta y_{i,u}, \Delta z_{i,u}]^\top$ and $R_{i,u} = R_x(\Delta \phi_{i,u}) R_y(\Delta \theta_{i,u}) R_z(\Delta \psi_{i,u})$.
 253

254 The rotation order $R_x R_y R_z$ follows our implementation; if a world-frame (left-multiply) update or a
 255 different Euler order is used, the composition should be adjusted accordingly. Definition 4.1 therefore
 256 makes $\mathbf{p}_t = \pi(T_t)$ an explicit function of the full 7-DoF action sequence within each window.
 257

258 **Windowed trajectory distance.** Given \mathbf{p}_t from Def. 4.1, we quantify motion per window either by
 259 the Euclidean displacement:

$$260 \quad \delta_i = \sum_{t=b_i}^{e_i-1} \|\mathbf{p}_{t+1} - \mathbf{p}_t\|_2. \quad (15)$$

262 The windowed trajectory distance aims to yield a scalar δ_i that captures overall motion magnitude
 263 and subsequently drives our pruning decision rule.
 264

265 **Dynamic decision function.** Given a windowed trajectory distance, we define a binary state variable
 266 $s_i \in \{0, 1\}$, where $s_i = 0$ corresponds to the *full-vision* state (w/o pruning) and $s_i = 1$ to the *pruned*
 267 state (cross-attention pruning). therefore next state could be determined by

$$268 \quad s_{i+1} = f(\delta_i) = \begin{cases} 1, & \delta_i \geq \bar{\delta}_i, \\ 0, & \delta_i < \bar{\delta}_i; \end{cases} \quad \bar{\delta}_i = \frac{1}{i} \sum_{j=1}^i \delta_j. \quad (16)$$

270 The dynamic switch to s_{i+1} adapts to the global motion scale of the task, enabling pruning during
 271 periods of high activity while retaining full vision during fine-grained phases. An alternative is the
 272 *adjacent-extrema function*, which sets thresholds based on the extrema of the most recent τ windows:
 273

$$274 \quad U^{(i)} = \max\{\delta_{i-\tau+1}, \dots, \delta_i\}, \quad (17)$$

$$275 \quad V^{(i)} = \min\{\delta_{i-\tau+1}, \dots, \delta_i\}$$

276 with the update rule

$$278 \quad s_{i+1} = \begin{cases} 1, & \delta_i \geq U^{(i)}, \\ 279 \quad 0, & \delta_i \leq V^{(i)}, \\ 280 \quad s_i, & V^{(i)} < \delta_i < U^{(i)}. \end{cases} \quad (18)$$

281 This design aims to respond quickly to local motion variations, capturing abrupt efficient shifts
 282 between coarse and delicate manipulations. When the robot exhibits large-amplitude motions,
 283 pruning is activated to suppress redundant visual input and reduce computation. When motion
 284 amplitude decreases, signaling the onset of fine manipulation, pruning is disabled to preserve the
 285 complete visual context necessary for accurate control.
 286

287 4.3 THEORETICAL ANALYSIS OF COMPUTATIONAL COMPLEXITY

289 We consider the computational cost of the Transformer stack in f_{LLM} with respect to the sequence
 290 length before and after pruning. Let S denote the token length of the full multi-modal sequence
 291 in Eq. 2, D the hidden dimension, and M the intermediate dimension of the feed-forward network
 292 (SwiGLU). The total number of vision tokens before pruning is L_{vis} , while $k = \lfloor \rho \cdot L_{\text{vis}} \rfloor$ tokens are
 293 kept after the text-driven selection in Eq. 10. We denote by T the number of forwards in a complete
 294 task execution (Eq. 5), and by $\gamma \in [0, 1]$ the proportion of forwards executed in the pruned state
 295 (Sec. 4.2). Let H be the number of Transformer layers in f_{LLM} .

296 For one Transformer layer, the FLOPs are approximated by

$$297 \quad F(S; D, M) \approx 2S^2D + 4SD^2 + 6SDM, \quad (19)$$

299 corresponding to attention, projections, and MLP. A baseline forward of the H -layer LLM therefore
 300 costs

$$301 \quad F_{\text{base}} = H \cdot F(S; D, M). \quad (20)$$

303 In ADP, pruning happens *before* the LLM at the embedding stage: visual tokens are ranked and
 304 reduced using Eq. 9–10, yielding the shorter sequence

$$305 \quad S' = 1 + k + L_{\text{prop}} + L_{\text{txt}} + L_{\text{act}} + 1. \quad (21)$$

307 The scoring overhead uses lightweight projections and a similarity matrix between text and vision
 308 embeddings,

$$309 \quad F_{\text{score}} = 2L_{\text{txt}}D^2 + 2L_{\text{vis}}D^2 + 2N^h L_{\text{txt}}L_{\text{vis}}d. \quad (22)$$

310 Assume pruning and scoring are performed once per forward *before* any Transformer layer, so all
 311 H layers operate on S' , the per-layer cost follows $F(S; D, M) \approx 2S^2D + 4SD^2 + 6SDM$, and
 312 $D = N^h d$,

$$313 \quad \Delta F_{\text{ADP}} = F_{\text{base}} - F_{\text{ADP}}, \quad F_{\text{ADP}} = F_{\text{score}} + H \cdot F(S'; D, M), \quad (23)$$

314 where $k = \lfloor \rho L_{\text{vis}} \rfloor$, S' is as above with L_{prop} , L_{txt} , L_{act} the proprioception/text/action lengths, N^h is
 315 the number of attention heads of size d , and $F_{\text{base}} = H F(S; D, M)$. Over an episode of T forwards,
 316 the expected complexity under the dynamic strategy is
 317

$$318 \quad \mathbb{E}[\mathcal{F}_{\text{episode}}] = T(\gamma F_{\text{ADP}} + (1 - \gamma) F_{\text{base}}), \quad (24)$$

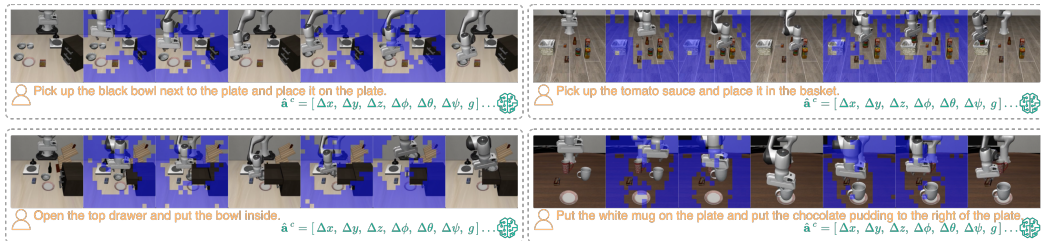
319 with expected savings

$$320 \quad \mathbb{E}[\Delta \mathcal{F}_{\text{episode}}] = T \gamma \Delta F_{\text{ADP}}. \quad (25)$$

322 The pruning is applied at the embedding stage prior to f_{LLM} , so the reduced length S' benefits all H
 323 layers uniformly, and the dynamic rule (Eq. 14–16) controls how often the pruned path is used across
 action windows.

324 **Table 1: Results on the LIBERO Benchmark.** **TR:** Training-Free; **AR:** Auto-Regressive; **PD:**
 325 Parallel Decoding. **Ratio:** The retain tokens / Full tokens.

Method	TR	Decoding	CKPT	Spatial	Object	Goal	Long	Average	FLOPs↓	Speedup↑
OpenVLA Kim et al. (2024)	-	AR	OpenVLA (7B)	84.7%	88.4%	79.2%	53.7%	76.5%	-	-
SparseVLM Zhang et al. (2024)	✓	AR	OpenVLA (7B)	79.8%	67.0%	72.6%	39.4%	64.7%	-	-
FastV Chen et al. (2024)	✓	AR	OpenVLA (7B)	83.4%	84.0%	74.2%	51.6%	73.3%	-	-
VLA-Cache Xu et al. (2025)	✓	AR	OpenVLA (7B)	83.8%	85.8%	76.4%	52.8%	74.7%	-	-
FlashVLA Tan et al. (2025)	✓	AR	OpenVLA (7B)	84.2%	86.4%	75.4%	51.4%	74.4%	-	-
SP-VLA Li et al. (2025)	✓	AR	OpenVLA (7B)	75.4%	85.6%	84.4%	54.2%	74.9%	-	-
WorldVLA Cen et al. (2025)	-	AR	Chameleon (7B)	85.6%	89.0%	82.6%	59.0%	79.1%	-	-
WorldVLA* Cen et al. (2025)	-	AR	Chameleon (7B)	87.6%	96.2%	83.4%	60.0%	81.8%	-	-
NORA Hung et al. (2025)	-	AR	Qwen-VL (3B)	85.6%	87.8%	77.0%	45.0%	73.9%	-	-
SmolVLM Shukor et al. (2025)	-	AR	SmolVLM (2.25B)	93.0%	94.0%	91.0%	77.0%	88.8%	-	-
CogACT Li et al. (2024)	-	FM	CogVLM (7B)	97.2%	98.0%	90.2%	88.8%	93.6%	-	-
NORA-Long Hung et al. (2025)	-	PD	Qwen-VL (3B)	92.2%	95.4%	89.4%	74.6%	87.9%	-	-
OpenVLA-OFT Kim et al. (2025)	-	PD	OFT (7B)	98.6%	98.2%	96.6%	94.8%	97.1%	7.91	1.00x
FastV(+OFT) Chen et al. (2024)	✓	PD	OFT (7B)	96.8%	81.0%	96.4%	73.0%	86.8%	6.37	1.24x
VLA-ADP (Ratio=30%)	✓	PD	OFT (7B)	97.6%	98.4%	97.4%	84.2%	94.4%	5.85	1.35x
VLA-ADP (Ratio=40%)	✓	PD	OFT (7B)	98.2%	97.2%	96.6%	87.2%	94.8%	6.14	1.29x
VLA-ADP (Ratio=50%)	✓	PD	OFT (7B)	99.4%	98.0%	96.4%	91.2%	96.3%	6.43	1.23x
VLA-ADP (Ratio=60%)	✓	PD	OFT (7B)	98.8%	98.0%	95.8%	92.0%	96.2%	6.74	1.17x
VLA-ADP (Ratio=70%)	✓	PD	OFT (7B)	99.0%	98.2%	96.8%	91.2%	96.3%	7.03	1.13x



340
 341
 342
 343
 344
 345
 346
 347
 348
 349 Figure 4: Visualisation of our method on representative examples of the four LIBERO task types
 350 (Spatial, Object, Goal, Long). Blue masks ■ indicate pruned vision tokens. The retained tokens
 351 consistently highlight task-relevant objects, validating the Text-driven Anticipatory Pruning. Moreover,
 352 full vision tokens are restored at critical phases (e.g., initialisation, grasping, placement), demon-
 353 strating the effectiveness of the Task-driven Pruning and Action-Aware Dynamic Strategy.

354 5 EXPERIMENTS

355 We conduct experiments across LIBERO simulation and real-robot tasks under standardized set-
 356 tings, comparing against strong baselines and conducting targeted ablations to assess success rates,
 357 compute/latency, and the contributions of dynamic scheduling and layer-wise pruning.

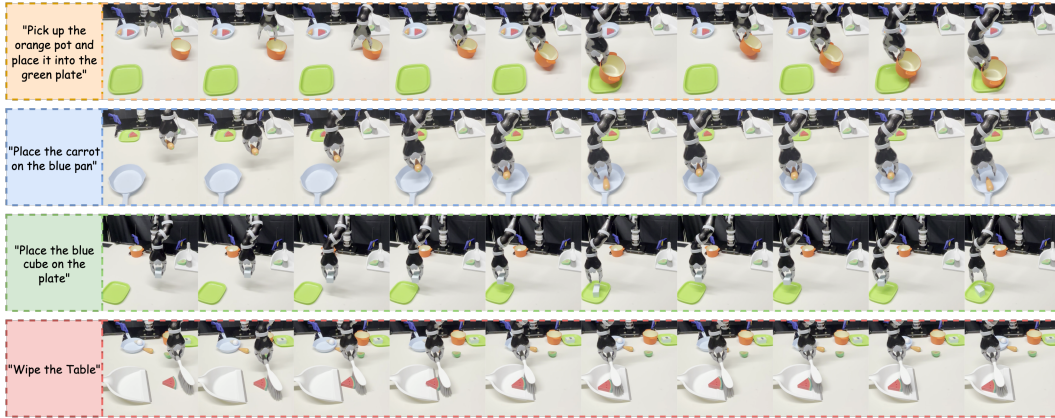
358 5.1 SIMULATION EXPERIMENTS

359 **Experiments setup.** For simulation, we use LIBERO Liu et al. (2023a) with four suites (*i.e.*, Spatial,
 360 Object, Goal, Long) evaluating spatial understanding, object recognition, goal-directed behaviour,
 361 and long-horizon planning. All Libero settings follow OpenVLA-OFT, using its public run scripts.
 362 For comparison, we reproduce FastV Chen et al. (2024) on OpenVLA-OFT and run under the same
 363 environment. Experiments run on Linux with an NVIDIA RTX 4090. We set the window size to
 364 the OpenVLA-OFT chunk size (8) and apply a cold start: the first two windows use full vision.
 365 To limit error accumulation, if pruning occurs in three consecutive windows, the next window is
 366 forced to full vision. In multi-view pruning, the main wrist retention is 4:6. Within the Action-Aware
 367 Dynamic Strategy, we use Euclidean displacement and the adjacent-extrema rule; in its third case we
 368 deterministically set the state to 1 (instead of inheriting s_i) to further reduce FLOPs.

369 **Main result.** Table 1 shows that VLA-ADP achieves a stable accuracy–compute trade-off across the
 370 keep ratio on LIBERO. Compared to OpenVLA-OFT, when the keep ratio is 50–70%, the average
 371 success rate slightly decreases ($\leq 0.9\%$), while the LLM-side inference speed improves by up to
 372 1.23x, and the FLOPs are markedly below the baseline. Further compressing the retention rate to
 373 30–40% maintains an average SR of 94.4–94.8%, yet attains 1.29–1.35x speedup. Notably, VLA-
 374 ADP achieves a 99.4% success rate on the Spatial, indicating that VLA-ADP successfully prunes
 375 redundant vision tokens while selectively preserving key information in relatively simple spatial

378
379
380
381 **Table 2: Real-World Experiments (4 tasks).** Task 1 to Task 4 cover the picking, placing and wiping
382 motion, which covering a variety of objects.
383
384

Method	Decoding	Task1	Task2	Task3	Task4	Average	Latency↓	Speedup↑
OpenVLA-OFT (base)	PD	83.3%	93.3%	86.7%	80.0%	85.8%	76.9	1.00
VLA-ADP (ours)	PD	90.0%	90.0%	90.0%	83.3%	88.3%	51.8	1.49×



385
386
387
388
389
390
391
392
393
394
395
396
397
398
399 **Figure 5: Real world experiments.** We conduct the experiments on Jaco2 Real-world Platform.
400

401 manipulation scenarios. By contrast, Random Dropping (50%) yields a 1.29× speedup on the LLM
402 side and performs reasonably on the Spatial and Goal, but its success rates on Object and Long are
403 only 73.0% and 76.2%, respectively.

404 5.2 REAL-WORLD EXPERIMENTS

405 **Experiment setup.** We evaluate on four real tasks executed on a physical robot: *Task1*: pick up
406 the orange pot and place it in the green plate; *Task2*: place the blue cube on the plate; *Task3*: place
407 the carrot on the blue pan; *Task4*: wipe the table. All runtime settings mirror the simulation: Linux
408 workstation with an NVIDIA RTX 4090, parallel decoding (PD) and window size equal to OpenVLA-
409 OFT chunk size (8) with a two-window cold start (full vision). To curb error accumulation, if pruning
410 is enabled for three consecutive windows, the next window uses full vision. Within the Action-Aware
411 Dynamic Strategy we use Euclidean displacement and the adjacent-extrema rule, and in the third case
412 deterministically set the state to 1 to further reduce FLOPs.

413 **Main result.** Table 2 summarizes the outcomes. VLA-ADP improves the average success rate
414 from 85.8% to 88.3% while reducing latency from 76.9 to 51.8 (baseline/ours = **1.49×**). Per task,
415 VLA-ADP outperforms the baseline on Task1/3/4 (90.0%, 90.0%, 83.3%) and is still competitive on
416 Task2 (90.0% vs. 93.3%). These results indicate that our dynamic pruning maintains or improves
417 real-world success while yielding substantial speedup.

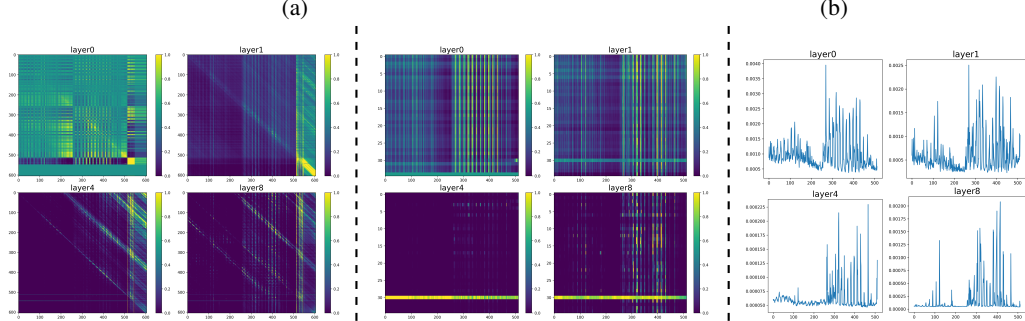
420 6 ABLATION STUDY

421 We conduct ablations on each component of our method: first removing the dynamic strategy to test
422 ADP (*w/o Action-aware Dynamic*); then ablating the pruning module (*w/o Text-driven Pruning*) with
423 different weight selections for relevance scoring.

424 **Action-aware Dynamic Strategy.** We assess the impact of the dynamic strategy with two baselines:
425 removing the dynamic function (*ADP w/o D*) and a handcrafted periodic switching variant (*w/o
426 D + PS*). Table 3a (a) shows that introducing the dynamic controller (ADP) yields the best overall
427 accuracy-compute balance: 96.3% average SR with $\rho^{avg} = 0.22$ and 6.43 FLOPs, outperforming
428 the variant *w/o D* (93.45%, $\rho^{avg} = 0.25$, 6.23 FLOPs) and the periodic schedule *w/o D + PS* (89.9%,
429 $\rho^{avg} = 0.50$, 4.55 FLOPs). Per-suite, the dynamic policy preserves Goal/Long while boosting
430 Spatial/Object—most notably a **+16.6** point gain on *Object* over the periodic schedule (98.0% vs.
431

432 **Table 3: Ablation Study on each component of our design. (a)** Ablation on dynamic strategies (f).
433 **(b)** Ablation on pruning based on weights retrieved from layer l . Metrics are SR (%) and FLOPs.
434

f	Spatial	Object	Goal	Long	Avg			l	Spatial	Object	Goal	Long	Avg		
	SR↑	SR↑	SR↑	SR↑	SR↑	ρ^{avg}	FLOPs↓		SR↑	SR↑	SR↑	SR↑	SR↑	FLOPs↓	
ADP	99.4%	98.0%	96.4%	91.2%	96.3%	0.22	6.43	0	99.4%	98.0%	96.4%	91.2%	96.3%	6.43	
- w/o D	98.2%	88.0%	96.4%	91.2%	93.45%	0.25	6.23	1	98.2%	97.6%	96.2%	89.8%	95.5%	6.57	
- w/o D + PS	95.0%	81.4%	96.2%	87.0%	89.9%	0.50	4.55	4	98.0%	97.8%	96.4%	91.2%	95.8%	6.89	



450 (a) Original Attention Maps (b) Pruning Attention Maps. (c) Vision tokens importance score.
451 Figure 6: The figure illustrates the layer-wise importance score of the vision tokens. (a) Vision–vision
452 self-similarity (across layers) (b) Text→vision attention (after ADP) (c) Vision-token importance Φ
453

454 81.4%), and **+4.4** on *Spatial* (99.4% vs. 95.0%). Compared to *ADP w/o D*, *ADP* improves average
455 SR by **+2.85** points with comparable compute (+0.20 FLOPs), indicating that state-aware switching
456 (rather than fixed cycling) is crucial to avoid over-pruning during fine manipulation while still pruning
457 aggressively when large motions occur.

458 **Impact of Pruning Strategy.** We ablate layer selection to validate using layer 0 for importance
459 scoring. Table 3b (b) shows that final SR is similar across layers, with layer 0 yielding the best
460 accuracy–compute balance: 96.3% average SR with 6.43 FLOPs, compared to layer 1 (95.5%, 6.57
461 FLOPs) and layer 4 (95.8%, 6.89 FLOPs). Meanwhile, FLOPs increase with deeper layers, so
462 selecting $l = 0$ offers a superior performance–efficiency trade-off. The slight decline in average SR
463 with depth corroborates our analysis: deeper layers induce more localised attention—sharpening
464 peaks vs. non-peaks but reducing global state coverage—thus becoming more sensitive to occasional
465 mismatches and noise, which leads to marginally lower success rates.

466 **Observation of Attention Weights.** A common view holds that text–vision alignment concentrates
467 in deeper multimodal layers, so high importance scores should be computed there; however, this need
468 not hold for parallel-decoding VLA. Our visualizations and measurements show that layer 0 already
469 provides a stable, discriminative text-to-vision signal. In Fig. 6a, the layer-0 self-similarity matrix
470 shows a clear high-contrast block structure, while deeper layers become increasingly diagonal-banded,
471 compressing non-local correlations. The text to vision submatrix (Fig. 6b) follows the same trend:
472 layer 0 exhibits pronounced peaks and troughs across many vision tokens, whereas deeper layers
473 retain only a few narrow high-response bands. The token importance score Φ (Fig. 6c) likewise has
474 higher SNR at layer 0; with depth, curves sharpen and develop long tails or near collapse, making
475 top- k ranking more sensitive to local noise.

7 CONCLUSION

480 We presented VLA-ADP, a plug-and-play pruning framework that unifies text-driven anticipatory
481 pruning with an action-aware dynamic strategy to accelerate VLA inference while preserving reliabil-
482 ity. Across simulation and real-world evaluations, the method maintains or improves task success,
483 reduces compute, and shortens inference latency. The dynamic controller consistently outperforms
484 removal and periodic switching, and early-layer scoring offers the best accuracy–efficiency balance.
485 These results indicate that adaptively pruning vision tokens by motion state and instruction relevance
486 enables efficient, fine-grained manipulation without compromising control quality.

486 REFERENCES
487

488 Anas Awadalla, Irena Gao, Josh Gardner, Jack Hessel, Yusuf Hanafy, Wanrong Zhu, Kalyani Marathe,
489 Yonatan Bitton, Samir Gadre, Shiori Sagawa, et al. Openflamingo: An open-source framework for
490 training large autoregressive vision-language models. *arXiv preprint arXiv:2308.01390*, 2023.

491 Johan Bjorck, Fernando Castañeda, Nikita Cherniadev, Xingye Da, Runyu Ding, Linxi Fan, Yu Fang,
492 Dieter Fox, Fengyuan Hu, Spencer Huang, et al. Gr0ot n1: An open foundation model for generalist
493 humanoid robots. *arXiv preprint arXiv:2503.14734*, 2025.

494

495 Kevin Black, Noah Brown, Danny Driess, Adnan Esmail, Michael Equi, Chelsea Finn, Niccolò
496 Fusai, Lachy Groom, Karol Hausman, Brian Ichter, et al. A vision-language-action flow model for
497 general robot control. *arXiv preprint arXiv:2410.24164*, 2024.

498

499 Anthony Brohan, Noah Brown, Justice Carbajal, Yevgen Chebotar, Xi Chen, Krzysztof Choromanski,
500 Tianli Ding, Danny Driess, Avinava Dubey, Chelsea Finn, et al. Rt-2: Vision-language-action
501 models transfer web knowledge to robotic control, 2023. URL <https://arxiv.org/abs/2307.15818>,
502 2024.

503

504 Jun Cen, Chaohui Yu, Hangjie Yuan, Yuming Jiang, Siteng Huang, Jiayan Guo, Xin Li, Yibing Song,
505 Hao Luo, Fan Wang, et al. Worldvla: Towards autoregressive action world model. *arXiv preprint
arXiv:2506.21539*, 2025.

506

507 Liang Chen, Haozhe Zhao, Tianyu Liu, Shuai Bai, Junyang Lin, Chang Zhou, and Baobao Chang.
508 An image is worth 1/2 tokens after layer 2: Plug-and-play inference acceleration for large vision-
509 language models. In *European Conference on Computer Vision*, pp. 19–35. Springer, 2024.

510

511 Cheng Chi, Zhenjia Xu, Siyuan Feng, Eric Cousineau, Yilun Du, Benjamin Burchfiel, Russ Tedrake,
512 and Shuran Song. Diffusion policy: Visuomotor policy learning via action diffusion. *The
International Journal of Robotics Research*, pp. 02783649241273668, 2023.

513

514 Chia-Yu Hung, Qi Sun, Pengfei Hong, Amir Zadeh, Chuan Li, U Tan, Navonil Majumder, Soujanya
515 Poria, et al. Nora: A small open-sourced generalist vision language action model for embodied
516 tasks. *arXiv preprint arXiv:2504.19854*, 2025.

517

518 Moo Jin Kim, Karl Pertsch, Siddharth Karamcheti, Ted Xiao, Ashwin Balakrishna, Suraj Nair,
519 Rafael Rafailov, Ethan Foster, Grace Lam, Pannag Sanketi, et al. Openvla: An open-source
520 vision-language-action model. *arXiv preprint arXiv:2406.09246*, 2024.

521

522 Moo Jin Kim, Chelsea Finn, and Percy Liang. Fine-tuning vision-language-action models: Optimizing
523 speed and success. *arXiv preprint arXiv:2502.19645*, 2025.

523

524 Qixiu Li, Yaobo Liang, Zeyu Wang, Lin Luo, Xi Chen, Mozheng Liao, Fangyun Wei, Yu Deng,
525 Sicheng Xu, Yizhong Zhang, et al. Cogact: A foundational vision-language-action model for
526 synergizing cognition and action in robotic manipulation. *arXiv preprint arXiv:2411.19650*, 2024.

527

528 Ye Li, Yuan Meng, Zewen Sun, Kangye Ji, Chen Tang, Jiajun Fan, Xinzhu Ma, Shutao Xia, Zhi
529 Wang, and Wenwu Zhu. Sp-vla: A joint model scheduling and token pruning approach for vla
model acceleration. *arXiv preprint arXiv:2506.12723*, 2025.

530

531 Bo Liu, Yifeng Zhu, Chongkai Gao, Yihao Feng, Qiang Liu, Yuke Zhu, and Peter Stone. Libero:
532 Benchmarking knowledge transfer for lifelong robot learning. *Advances in Neural Information
Processing Systems*, 36:44776–44791, 2023a.

533

534 Haotian Liu, Chunyuan Li, Yuheng Li, and Yong Jae Lee. Improved baselines with visual instruction
535 tuning, 2023b.

536

537 Haotian Liu, Chunyuan Li, Qingyang Wu, and Yong Jae Lee. Visual instruction tuning, 2023c.

538

539 Haotian Liu, Chunyuan Li, Yuheng Li, Bo Li, Yuanhan Zhang, Sheng Shen, and Yong Jae Lee.
Llava-next: Improved reasoning, ocr, and world knowledge, January 2024a. URL <https://llava-vl.github.io/blog/2024-01-30-llava-next/>.

540 Jiaming Liu, Mengzhen Liu, Zhenyu Wang, Lily Lee, Kaichen Zhou, Pengju An, Senqiao Yang,
 541 Renrui Zhang, Yandong Guo, and Shanghang Zhang. Robomamba: Multimodal state space model
 542 for efficient robot reasoning and manipulation. *arXiv e-prints*, pp. arXiv–2406, 2024b.

543

544 Maxime Oquab, Timothée Darcet, Théo Moutakanni, Huy Vo, Marc Szafraniec, Vasil Khalidov,
 545 Pierre Fernandez, Daniel Haziza, Francisco Massa, Alaaeldin El-Nouby, et al. Dinov2: Learning
 546 robust visual features without supervision. *arXiv preprint arXiv:2304.07193*, 2023.

547

548 Mustafa Shukor, Dana Aubakirova, Francesco Capuano, Pepijn Kooijmans, Steven Palma, Adil Zouï-
 549 tine, Michel Aractingi, Caroline Pascal, Martino Russi, Andres Marafioti, et al. Smolvla: A vision-
 550 language-action model for affordable and efficient robotics. *arXiv preprint arXiv:2506.01844*,
 551 2025.

552

553 Xudong Tan, Yaxin Yang, Peng Ye, Jialin Zheng, Bizhe Bai, Xinyi Wang, Jia Hao, and Tao
 554 Chen. Think twice, act once: Token-aware compression and action reuse for efficient inference in
 555 vision-language-action models. *arXiv preprint arXiv:2505.21200*, 2025.

556

557 Gemini Team, Rohan Anil, Sebastian Borgeaud, Jean-Baptiste Alayrac, Jiahui Yu, Radu Soricut,
 558 Johan Schalkwyk, Andrew M Dai, Anja Hauth, Katie Millican, et al. Gemini: a family of highly
 559 capable multimodal models. *arXiv preprint arXiv:2312.11805*, 2023.

560

561 Hugo Touvron, Louis Martin, Kevin Stone, Peter Albert, Amjad Almahairi, Yasmine Babaei, Nikolay
 562 Bashlykov, Soumya Batra, Prajjwal Bhargava, Shruti Bhosale, et al. Llama 2: Open foundation
 563 and fine-tuned chat models. *arXiv preprint arXiv:2307.09288*, 2023.

564

565 Junjie Wen, Yichen Zhu, Jinming Li, Zhibin Tang, Chaomin Shen, and Feifei Feng. Dexvla:
 566 Vision-language model with plug-in diffusion expert for general robot control. *arXiv preprint
 567 arXiv:2502.05855*, 2025a.

568

569 Junjie Wen, Yichen Zhu, Minjie Zhu, Zhibin Tang, Jinming Li, Zhongyi Zhou, Xiaoyu Liu, Chaomin
 570 Shen, Yixin Peng, and Feifei Feng. Diffusionvla: Scaling robot foundation models via unified
 571 diffusion and autoregression. In *Forty-second International Conference on Machine Learning*,
 572 2025b.

573

574 Siyu Xu, Yunke Wang, Chenghao Xia, Dihao Zhu, Tao Huang, and Chang Xu. Vla-cache: Towards
 575 efficient vision-language-action model via adaptive token caching in robotic manipulation. *arXiv
 576 preprint arXiv:2502.02175*, 2025.

577

578 Yantai Yang, Yuhao Wang, Zichen Wen, Luo Zhongwei, Chang Zou, Zhipeng Zhang, Chuan Wen,
 579 and Linfeng Zhang. Efficientvla: Training-free acceleration and compression for vision-language-
 580 action models. *arXiv preprint arXiv:2506.10100*, 2025.

581

582 Yang Yue, Yulin Wang, Bingyi Kang, Yizeng Han, Shenzhi Wang, Shiji Song, Jiashi Feng, and Gao
 583 Huang. Deer-vla: Dynamic inference of multimodal large language models for efficient robot
 584 execution. *Advances in Neural Information Processing Systems*, 37:56619–56643, 2024.

585

586 Xiaohua Zhai, Basil Mustafa, Alexander Kolesnikov, and Lucas Beyer. Sigmoid loss for language
 587 image pre-training. In *Proceedings of the IEEE/CVF international conference on computer vision*,
 588 pp. 11975–11986, 2023.

589

590 Rongyu Zhang, Menghang Dong, Yuan Zhang, Liang Heng, Xiaowei Chi, Gaole Dai, Li Du, Yuan
 591 Du, and Shanghang Zhang. Mole-vla: Dynamic layer-skipping vision language action model via
 592 mixture-of-layers for efficient robot manipulation. *arXiv preprint arXiv:2503.20384*, 2025.

593

594 Yuan Zhang, Chun-Kai Fan, Junpeng Ma, Wenzhao Zheng, Tao Huang, Kuan Cheng, Denis Gu-
 595 dovskiy, Tomoyuki Okuno, Yohei Nakata, Kurt Keutzer, et al. Sparsevlm: Visual token sparsifica-
 596 tion for efficient vision-language model inference. *arXiv preprint arXiv:2410.04417*, 2024.

594 APPENDIX

595
596 THE USE OF LARGE LANGUAGE MODELS597
598 In this manuscript, we used a LLM as a writing assistant to refine the presentation of certain contents.
599 Specifically, the LLM was used to: (1) Rephrase sentences and paragraphs for greater readability,
600 conciseness, and academic formality. (2) Correct grammar, spelling, and punctuation errors. (3)
601 Improve logical flow and transitions between sentences. All content enhanced by the LLM has been
602 thoroughly reviewed by the authors to ensure accuracy. The core idea, technical contributions, and
603 results of the experiment are entirely the original contributions of the authors.

604 ALGORITHM

605
606 Here we provide the full pipeline of our proposed action-aware dynamic pruning for vision-language-
607 action models.608
609 **Algorithm 1** Action-Aware Dynamic Pruning (ADP) for VLA Inference610
611 **Require:** Multimodal embeddings $\mathbf{X}^m = [\mathbf{X}^{[BOS]}, \mathbf{X}^{vis}, \mathbf{X}^{prop}, \mathbf{X}^{txt}, \mathbf{X}^{act}, \mathbf{X}^{[EOS]}]$,
612 Q/K weights $W_Q^{(0)}, W_K^{(0)}$, retention ratio ρ , view weights $\alpha \in \mathbb{R}^C$ with $\sum_c \alpha_c = 1$,
613 gating rule $f(\cdot)$ (mean or adjacent-extrema), windowed actions \mathbf{A}_i^c , pose T_{b_i}
614
615 **Output:** Per-window visual state $s_i \in \{0, 1\}$, pruned sequence $\tilde{\mathbf{X}}^m$, actions $\hat{\mathbf{a}}$
616 1: **Init:** $s_1 \leftarrow 0$ (cold start, full vision), $s_2 \leftarrow 0$; $consec \leftarrow 0$ ▷ two-window cold start
617 2: **for** window $i = 1, 2, \dots$ **do**
618 3: **Compute windowed motion** δ_i via FK on \mathbf{A}_i^c (Def. 4.1):
619
$$\delta_i \leftarrow \sum_{t=b_i}^{e_i-1} \|\mathbf{p}_{t+1} - \mathbf{p}_t\|_2 \quad \text{with } \mathbf{p}_t = \pi(T_t), T_{t+1} = T_t \begin{bmatrix} R_{i,u} & \mathbf{v}_{i,u} \\ \mathbf{0}^\top & 1 \end{bmatrix}$$

620
621 4: **Gate update:** $s_{i+1} \leftarrow f(\delta_i)$
622 5: **if** $consec \geq 3$ **then** ▷ reset to avoid prolonged pruning
623 6: $s_{i+1} \leftarrow 0$; $consec \leftarrow 0$
624
625 7: **Branch by state**
626 8: **if** $s_{i+1} = 1$ **then** ▷ pruned path
627 9: **Q/K scoring at layer 0:**
628 10: $\mathbf{Q}^{(0)} = \mathbf{H}_{txt}^{(0)} W_Q^{(0)}, \mathbf{K}^{(0)} = \mathbf{H}_{vis}^{(0)} W_K^{(0)}, \mathbf{A}^{(0)} = \frac{\mathbf{Q}^{(0)} (\mathbf{K}^{(0)})^\top}{\sqrt{d}}$
629 11: **Aggregate importance** (Eq. 9): $\Phi^{(0)}(v) \leftarrow \frac{1}{N^h L_{txt}} \sum_{h,t} \mathbf{A}_{h,t,v}^{(0)}$
630 12: $k \leftarrow \lfloor \rho \cdot L^{vis} \rfloor$; $k_c \leftarrow \lfloor \alpha_c \cdot k \rfloor$ for $c=1..C$
631 13: **Per-view Top- k :** $\mathbf{X}_{(c)}^{vis} \leftarrow \text{Top-K}(\Phi_{(c)}^{(0)}, k_c)$; $\mathbf{X}_{keep}^{vis} \leftarrow \bigcup_c \mathbf{X}_{(c)}^{vis}$
632 14: **Form pruned input:** $\tilde{\mathbf{X}}^m \leftarrow [\mathbf{X}^{[BOS]}, \mathbf{X}_{keep}^{vis}, \mathbf{X}^{prop}, \mathbf{X}^{txt}, \mathbf{X}^{act}, \mathbf{X}^{[EOS]}]$
633
634 15: **LLM forward:** $\hat{\mathbf{a}} \leftarrow f_{LLM}(\tilde{\mathbf{X}}^m)$; $consec \leftarrow consec + 1$
635
636 16: **else** ▷ full-vision path
637 17: **Execute** $\hat{\mathbf{a}}$ and advance to next window
638 18: **return** $\{s_i\}, \tilde{\mathbf{X}}^m, \hat{\mathbf{a}}$ 640
641 REAL-WORLD EXPERIMENT DETAILS642
643 We provide additional details of the real-robot experiments to facilitate reproducibility.644
645 **Robot Platform.** All real-world evaluations were conducted on a **Kinova Jaco2** 6-DoF robotic arm
646 equipped with a parallel-jaw gripper. The robot was controlled through Cartesian velocity commands
647 at 10 Hz, with joint and workspace safety limits enforced to prevent collisions.

648 **Sensing Setup.** A single RGB camera (Sony AX53) was mounted in front of the table to capture
 649 the entire workspace. The camera streamed RGB frames at 640×480 resolution and 30 FPS. No
 650 wrist-mounted camera was used in the real-robot experiments, and all observations were obtained
 651 from this fixed view.
 652

653 **Runtime Environment.** All policies were executed on a Linux workstation running Ubuntu 20.04
 654 with an NVIDIA RTX 4090 GPU. Inference employed parallel decoding with an OFT chunk size of
 655 8. Latency was measured as mean per-step inference time over 100 runs.
 656

657 **Task Setup.** We evaluated four tabletop manipulation tasks: **a) Task 1:** Pick up the orange pot
 658 and place it into a green plate. **b) Task 2:** Pick and place a blue cube onto the plate. **c) Task 3:**
 659 Pick and place a carrot into a blue pan. **d) Task 4:** Wipe the table. Objects were placed randomly
 660 within a 50×50 cm workspace area at the beginning of each trial. For data collection, each task was
 661 executed using a gamepad teleoperation interface, with the human operator directly controlling the
 662 Jaco2 arm. We collected approximately 100–150 trajectories per task, covering diverse initial states
 663 and object positions. The collected demonstrations were then used to build the training dataset, and
 664 we fine-tuned OpenVLA-OFT separately on each task before deploying the model for evaluation in
 665 the real-robot experiments.
 666

667 **Evaluation Protocol.** Each task was repeated 30 trials under randomized object initializations.
 668 A trial was marked as successful if the object was placed entirely within the target receptacle (for
 669 Tasks 1–3) or if more than 80% of the designated area was wiped (Task 4). At the end of each episode,
 670 the robot was reset to a neutral home pose. Safety termination was triggered if joint torque exceeded
 671 preset thresholds.
 672

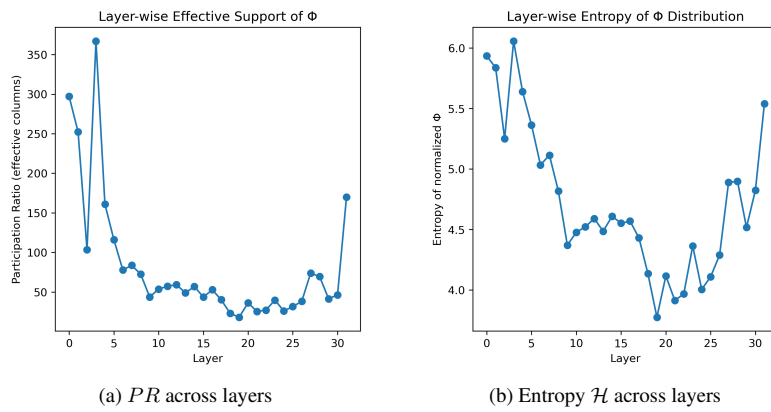
672 QUANTITATIVE STATISTICS

673 To complement the attention visualizations with comparable quantitative evidence, we compute
 674 scale-free statistics at each layer from the text-to-vision importance vector $\Phi = \{\phi_i\}_{i=1}^V$. We first
 675 normalize Φ as $p_i = \phi_i / \sum_{j=1}^V \phi_j$ and then evaluate the *Participation Ratio (PR)* and the *Entropy*
 676 (\mathcal{H}):
 677

$$678 \quad PR = \frac{1}{\sum_{i=1}^V p_i^2}, \quad \mathcal{H}(p) = - \sum_{i=1}^V p_i \log p_i. \quad (26)$$

679 PR approximates the effective number of participating visual columns, while \mathcal{H} quantifies the
 680 dispersion and multi-modality of the distribution. Together, they characterize the spatial coverage of
 681 alignment signals and the stability of Top- K ranking.
 682

683 Figure 7a presents the variation of PR across layers. In shallow layers, PR remains relatively high,
 684 indicating that a large number of key vision tokens receive balanced attention and contribute to broad
 685 spatial coverage. As depth increases, PR rapidly decreases and stabilizes, reflecting a progressive
 686 collapse of attention onto a small subset of tokens and reduced feature utilization.
 687



691 **Figure 7: Layer-wise statistics of text-to-vision importance scores.**

Figure 7b presents the corresponding entropy \mathcal{H} across layers. Shallow layers exhibit higher entropy, suggesting diverse and smooth distributions that make Top- K selection robust against individual outliers. In contrast, deeper layers display sharply peaked distributions dominated by a few tokens. While such localization may benefit semantic alignment in downstream reasoning, it renders Top- K selection unstable and prone to discarding critical tokens. These findings suggest that shallow-layer attention signals are preferable for estimating the importance of vision tokens in VLA tasks. In particular, using layer-0 offers a computationally efficient choice, providing reliable importance estimates while further reducing FLOPs.

RANDOM PRUNING COMPARISON

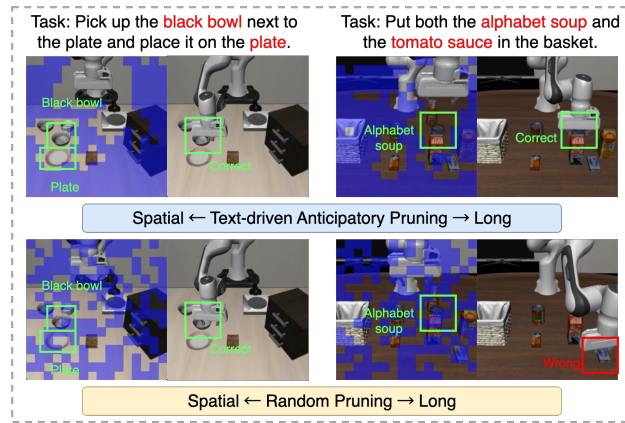


Figure 8: ADP (Text-Driven Pruning) vs. Random Pruning.

Random Pruning yields competitive performance on Spatial and Goal, but performs substantially worse on Object and Long. We can attribute this phenomenon to the distribution of visual patches spanned by the key object as shown in Figure 8. When the target object spans a large number of patches, random pruning still has a high probability of retaining the relevant patches, thereby preserving sufficient task-critical vision information. In contrast, random pruning is more likely to prune the relevant patches when the key object spans only a small number of patches. Such pruning may result in incorrect object identification, which in turn propagates errors and ultimately causes task failure.

INVERSION EXPERIMENT

Table 4: Inversion Experiment.

Task	Keep Ratio=30%			Keep Ratio=50%			Keep Ratio=70%		
	Direct	Inverse	Gap	Direct	Inverse	Gap	Direct	Inverse	Gap
Spatial	97.6%	44.0%	53.6%	99.4%	54.8%	44.6%	99.0%	90.8%	8.2%
Object	98.4%	0.6%	97.8%	98.0%	11.8%	86.2%	98.2%	59.6%	38.6%
Goal	97.4%	43.6%	53.8%	96.4%	63.6%	32.8%	96.8%	84.8%	12.0%
Long	84.2%	0.2%	84.0%	91.2%	8.2%	83.0%	91.2%	37.4%	53.8%
Avg	94.4%	22.1%	72.3%	96.3%	34.6%	61.7%	96.3%	68.1%	28.1%

To further evaluate the reliability of our text-driven importance scores, we design a counterfactual inverse-pruning experiment that mirrors the full setup of the main results. Instead of retaining the most relevant visual tokens identified by our text–vision relevance ranking, we intentionally preserve the least relevant ones, while keeping all other factors, including model, hyperparameters, tasks, and ratios (30%, 50%, 70%), unchanged. If the relevance ranking were noisy or poorly aligned with task semantics, the performance gap between direct and inverse pruning would be small. Conversely,

756 a large and systematic divergence would indicate that the scoring mechanism faithfully captures
 757 task-relevant visual information.

759 The results in Table 4 show a clear and consistent separation between the two settings across all suites
 760 and keep ratios. Under a 30% keep ratio, the average success rate drops sharply from 94.4% (direct)
 761 to 22.1% (inverse), with near-complete failure on Object (0.6%) and Long (0.2%). Similar trends
 762 persist at 50% (from 96.3% to 34.6%) and 70% (from 96.3% to 68.1%). Notably, inverse-70% still
 763 performs far worse than direct-30%, highlighting that semantic relevance dominates task performance
 764 over the number of retained tokens.

765 Noteably, the degradation is particularly pronounced on Object and Long, which require fine-grained
 766 spatial reasoning and long-horizon planning. Under inverse pruning, the model effectively loses
 767 access to the high-ranked, task-relevant visual tokens used for object grounding, spatial reasoning,
 768 and contact-rich motion planning. This confirms that our importance scores do not drift toward
 769 irrelevant regions but consistently identify and prioritise semantically aligned visual tokens.

770 Taken together, these counterfactual results provide strong evidence that:

- 771 1. Task-relevant visual tokens play a decisive role in VLA tasks, and task success depends
 772 far more on preserving these semantically aligned tokens than on the number of tokens
 773 retained. Task performance collapses as soon as these high-relevance tokens are removed,
 774 demonstrating that semantic alignment is the dominant factor governing model behaviour.
- 775 2. The text-driven relevance scoring mechanism accurately identifies and prioritises essential
 776 visual tokens, showing that ADP’s anticipatory pruning relies on a stable and meaningful
 777 semantic signal rather than incidental attention fluctuations. The scoring module effectively
 778 captures the alignment between the task instruction and the image observations, precisely
 779 identifying the visual patches critical for object grounding, spatial reasoning, and contact-
 780 rich manipulation.

782 COMPUTATIONAL TRADE-OFF ANALYSIS

784 Table 5: FLOPs and speedup with keep ratio 0.3. ADP(i) denotes pruning based on the weights from
 785 the i-th layer.

787 Item	baseline	ADP (0)	ADP (2)	ADP (4)	ADP (8)	ADP (16)	ADP (24)
788 Keep Ratio	1.0	0.3	0.3	0.3	0.3	0.3	0.3
789 Scoring Layer	–	0	2	4	8	16	24
790 Seq. Len.	603	245	245	245	245	245	245
791 Vis. Tokens (kept)	512	154	154	154	154	154	154
792 Scoring FLOPs (T)	0.00	0.02	0.51	1.01	1.99	3.97	5.95
793 LLM FLOPs (T)	7.91	3.19	3.19	3.19	3.19	3.19	3.19
794 Total FLOPs (T)	7.91	3.21	3.70	4.20	5.18	7.16	9.14
795 Expected FLOPs (T)	7.91	5.85	6.06	6.27	6.71	7.58	8.45
796 Speedup (Orig/Exp.)	1.00	1.35	1.31	1.26	1.18	1.04	0.94

797 Table 6: FLOPs and speedup with keep ratio 0.4. ADP(i) denotes pruning based on the weights from
 798 the i-th layer.

801 Item	baseline	ADP (0)	ADP (2)	ADP (4)	ADP (8)	ADP (16)	ADP (24)
802 Keep Ratio	1.0	0.4	0.4	0.4	0.4	0.4	0.4
803 Scoring Layer	–	0	2	4	8	16	24
804 Seq. Len.	603	296	296	296	296	296	296
805 Vis. Tokens (kept)	512	205	205	205	205	205	205
806 Scoring FLOPs (T)	0.00	0.02	0.51	1.01	1.99	3.97	5.95
807 LLM FLOPs (T)	7.91	3.86	3.86	3.86	3.86	3.86	3.86
808 Total FLOPs (T)	7.91	3.88	4.37	4.86	5.85	7.83	9.80
809 Expected FLOPs (T)	7.91	6.14	6.35	6.57	7.00	7.87	8.74
810 Speedup (Orig/Exp.)	1.00	1.29	1.25	1.20	1.13	1.00	0.90

810
811
812
Table 7: FLOPs and speedup with keep ratio 0.5. ADP(i) denotes pruning based on the weights from
the i-th layer.
813

Item	baseline	ADP (0)	ADP (2)	ADP (4)	ADP (8)	ADP (16)	ADP (24)
Keep Ratio	1.0	0.5	0.5	0.5	0.5	0.5	0.5
Scoring Layer	–	0	2	4	8	16	24
Seq. Len.	603	347	347	347	347	347	347
Vis. Tokens (kept)	512	256	256	256	256	256	256
Scoring FLOPs (T)	0.00	0.02	0.51	1.01	1.99	3.97	5.95
LLM FLOPs (T)	7.91	4.53	4.53	4.53	4.53	4.53	4.53
Total FLOPs (T)	7.91	4.55	5.04	5.53	6.52	8.50	10.47
Expected FLOPs (T)	7.91	6.43	6.64	6.89	7.30	8.17	9.04
Speedup (Orig/Exp.)	1.00	1.23	1.19	1.15	1.08	0.97	0.87

823
824
Table 8: FLOPs and speedup with keep ratio 0.6.
825

Item	baseline	ADP (0)	ADP (2)	ADP (4)	ADP (8)	ADP (16)	ADP (24)
Keep Ratio	1.0	0.6	0.6	0.6	0.6	0.6	0.6
Scoring Layer	–	0	2	4	8	16	24
Seq. Len.	603	399	399	399	399	399	399
Vis. Tokens (kept)	512	308	308	308	308	308	308
Scoring FLOPs (T)	0.00	0.02	0.51	1.01	1.99	3.97	5.95
LLM FLOPs (T)	7.91	5.21	5.21	5.21	5.21	5.21	5.21
Total FLOPs (T)	7.91	5.23	5.72	6.22	7.20	9.18	11.16
Expected FLOPs (T)	7.91	6.74	6.94	7.16	7.60	8.47	9.34
Speedup (Orig/Exp.)	1.00	1.17	1.14	1.10	1.04	0.93	0.85

835
836
837 TRADE-OFF OF PRUNING.
838

839 To quantify the computational trade-off introduced by anticipatory pruning, we evaluate the FLOPs
840 associated with importance scoring and compare them against the savings obtained from reducing the
841 LLM sequence length. Tables 5-9 report detailed FLOPs measurements across a range of keep ratios
842 and scoring layers (all FLOPs reported in this section are computed under the original multimodal
843 sequence length of $S = 603$.)

844 Across all practically meaningful configurations, the scoring cost remains substantially smaller than
845 the compute saved by pruning. When importance ranking is performed using shallow layers (e.g.
846 layers 0–4), the scoring overhead remains within 0.02–1.01T FLOPs. In contrast, shortening the
847 visual sequence reduces the LLM compute from 7.91T to approximately 3.19–5.90T, yielding a 2–4T
848 reduction. The net effect is therefore dominated by the savings from operating on a shorter sequence,
849 and the overall inference cost decreases consistently.

850 When combined with the action-aware dynamic gating strategy, the expected inference cost reflects the
851 mixture of pruned and full-vision windows. In our implementation, the dynamic gate activates pruning
852 for roughly 44% of windows on average across LIBERO. Under this regime, the expected FLOPs per
853 forward become 5.85T (keep=0.3), 6.14T (keep=0.4), and 6.43T (keep=0.5), corresponding to 1.35 \times ,
854 1.29 \times , and 1.23 \times speedup over the baseline. These values already account for the scoring overhead,
855 confirming that the computational benefit persists under realistic usage.

856
857 OBSERVATION ON GATING RULES.
858

859 We also observe that performing relevance scoring at excessively deep layers (≥ 16) increases the
860 overhead to 3.97–5.95T FLOPs, which approaches or surpasses the FLOPs saved by pruning. In
861 such cases, the net speedup degrades and may even become slightly negative. However, this config is
862 not required in practice. Our ablation study already shows that layer-0 scoring not only minimises
863 computational overhead but also provides the most reliable and stable importance estimates, making
it the default choice in all experiments.

864
865
866 Table 9: FLOPs and speedup with keep ratio 0.7.
867
868
869
870
871
872
873
874
875
876
877
878
879
880
881
882
883
884
885
886
887
888
889
890
891
892
893
894
895
896
897
898
899
900
901
902
903
904
905
906
907
908
909
910
911
912
913
914
915
916
917
918

Item	baseline	ADP (0)	ADP (2)	ADP (4)	ADP (8)	ADP (16)	ADP (24)
Keep Ratio	1.0	0.7	0.7	0.7	0.7	0.7	0.7
Scoring Layer	—	0	2	4	8	16	24
Seq. Len.	603	450	450	450	450	450	450
Vis. Tokens (kept)	512	359	359	359	359	359	359
Scoring FLOPs (T)	0.00	0.02	0.51	1.01	1.99	3.97	5.95
LLM FLOPs (T)	7.91	5.88	5.88	5.88	5.88	5.88	5.88
Total FLOPs (T)	7.91	5.90	6.39	6.89	7.88	9.85	11.83
Expected FLOPs (T)	7.91	7.03	7.24	7.46	7.89	8.76	9.63
Speedup (Orig/Exp.)	1.00	1.13	1.09	1.06	1.00	0.90	0.82

Overall, the additional scoring computation is far smaller than the savings achieved through reduced sequence length for all practical settings, and the use of shallow-layer scoring ensures that the trade-off remains consistently positive. These results verify that the proposed pruning strategy offers genuine computational benefits without compromising performance.

CASE DISCUSSIONS

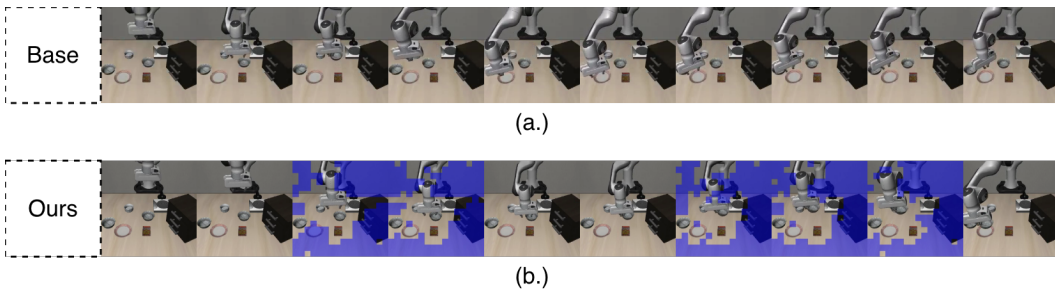


Figure 9: Baseline Failed but Ours Success on #Episode 110 of Spatial task.

OBSERVATION ON INTRIGUING PHENOMENON.

We observe an intriguing phenomenon: in several scenarios, the pruned model performs even better than the original baseline. To better understand this behavior, we further examine representative cases and analyze the underlying factors that contribute to such improvements. We identify a representative case that illustrates why moderate pruning can outperform the unpruned baseline. In Figure. 9 (a), the baseline model fails to grasp the bowl, whereas in Figure. 9 (b) our ADP method succeeds with a stable grasp. A closer inspection shows that the baseline allocates non-trivial attention to large, static background surfaces, effectively behaving like “sink” regions that dilute focus. After pruning these low-value background tokens, the model concentrates its attention on the immediate manipulation region—specifically the bowl and its supporting surface. This reduction of peripheral noise results in a more discriminative and task-aligned visual representation, helping the policy make more precise action decisions. Thus, in cases where background clutter dominates the unpruned attention distribution, pruning can improve operational focus and lead to higher success rates than the original baseline.

In addition to the individual cases discussed above, we further examined the per-task performance differences between ADP (keep ratio 0.5) and the OpenVLA-OFT baseline across all LIBERO suites, as reported in Tables 10–13. We observe that almost all degeneration are concentrated in the Long suite. In contrast, the Spatial, Object, and Goal suites remain largely unaffected, with success rates that are nearly identical to or slightly higher than the baseline. Notably, the most substantial degradations in the Long suite correspond to tasks with particularly long and compositional instructions, often involving multiple sequential subtasks. These tasks require the model to reallocate visual attention across distinct stages, each with its own set of relevant objects and fine-grained spatial relationships.



Figure 10: Per-stage curves drawn by Baseline and ADP.

Table 10: Spatial Suite Performance (ADP vs Baseline).

Task	Length	ADP	Baseline	Gap
pick up the black bowl between the plate and the ramekin and place it on the plate	82	100.0%	100.0%	0.0%
pick up the black bowl next to the ramekin and place it on the plate	68	100.0%	100.0%	0.0%
pick up the black bowl from table center and place it on the plate	66	100.0%	100.0%	0.0%
pick up the black bowl on the cookie box and place it on the plate	66	100.0%	98.0%	+2.0%
pick up the black bowl in the top drawer of the wooden cabinet and place it on the plate	88	98.0%	94.0%	+4.0%
pick up the black bowl on the ramekin and place it on the plate	63	98.0%	100.0%	-2.0%
pick up the black bowl next to the cookie box and place it on the plate	71	100.0%	100.0%	0.0%
pick up the black bowl on the stove and place it on the plate	61	98.0%	98.0%	0.0%
pick up the black bowl next to the plate and place it on the plate	66	100.0%	100.0%	0.0%
pick up the black bowl on the wooden cabinet and place it on the plate	70	100.0%	96.0%	+4.0%

Such behaviour reveals an intrinsic challenge of current VLA backbones. Since models like OpenVLA-OFT condition action generation solely on the current multi-modal sequence and static instruction, they lack explicit awareness of subtask completion. As a result, even after the first subgoal has been completed, the text-driven relevance scoring may continue to assign high importance to visual tokens associated with the earlier subgoal. Our inversion experiment demonstrated that VLA performance is extremely sensitive to the availability of correct visual tokens. Therefore, pruning under a limited token budget can amplify this issue, as tokens tied to an already completed subtask may still be retained due to textual relevance. In contrast, the subsequent subtask may receive insufficient visual coverage, which can ultimately lead to failure. These observations suggest that future progress may require enhancing VLA models with mechanisms for estimating subgoal progress or dynamically reallocating visual attention across long-horizon, multi-stage tasks.

IMPLEMENTATION DETAILS

Hyperparameters. We provide here the full set of hyperparameters used in our main experiments for reproducibility. These include all query–key (QK) pruning settings, dynamic gating parameters, and visualization options. Table 14 summarizes the exact values used in all results reported in the main text.

972
973
974
975
976
977
978
979
980
981
982
983
984
985
986
987
988
989
990
991
992
993
994
995
996
997
998
999
1000
1001
1002
1003
1004
1005
1006
1007
1008
1009
1010
1011
1012
1013
1014
1015
1016
1017
1018
1019
1020
1021
1022
1023
1024
1025
Table 11: Object Suite Performance (ADP vs Baseline).

Task	Length	ADP	Baseline	Gap
pick up the alphabet soup and place it in the basket	52	100.0%	98.0%	+2.0%
pick up the cream cheese and place it in the basket	51	100.0%	100.0%	0.0%
pick up the salad dressing and place it in the basket	53	98.0%	98.0%	0.0%
pick up the bbq sauce and place it in the basket	48	98.0%	100.0%	-2.0%
pick up the ketchup and place it in the basket	46	98.0%	100.0%	-2.0%
pick up the tomato sauce and place it in the basket	51	100.0%	100.0%	0.0%
pick up the butter and place it in the basket	45	96.0%	98.0%	-2.0%
pick up the milk and place it in the basket	43	98.0%	96.0%	+2.0%
pick up the chocolate pudding and place it in the basket	56	94.0%	92.0%	+2.0%
pick up the orange juice and place it in the basket	51	98.0%	100.0%	-2.0%

Table 12: Goal Suite Performance (ADP vs Baseline).

Task	Length	ADP	Baseline	Gap
open the middle drawer of the cabinet	37	100.0%	98.0%	+2.0%
put the bowl on the stove	25	94.0%	96.0%	-2.0%
put the wine bottle on top of the cabinet	41	94.0%	92.0%	+2.0%
open the top drawer and put the bowl inside	43	82.0%	88.0%	-6.0%
put the bowl on top of the cabinet	34	100.0%	100.0%	0.0%
push the plate to the front of the stove	40	98.0%	100.0%	-2.0%
put the cream cheese in the bowl	32	98.0%	96.0%	+2.0%
turn on the stove	17	100.0%	100.0%	0.0%
put the bowl on the plate	25	98.0%	98.0%	0.0%
put the wine bottle on the rack	31	100.0%	98.0%	+2.0%

Code Availability. Following the reviewer’s encouragement, we additionally provide a complete recipe of all hyperparameters, configuration files, and controller settings. Our implementation exposes all gating and pruning parameters through a unified configuration interface, making it easy to reproduce and extend the experiments (e.g., varying window sizes, pruning ratios, and similarity layers).

1026
1027
1028
1029
1030
1031
1032

Table 13: Long Suite Performance (ADP vs Baseline).

Task	Length	ADP	Baseline	Gap
put both the alphabet soup and the tomato sauce in the basket	61	94.0%	92.0%	+2.0%
put both the cream cheese box and the butter in the basket	58	96.0%	96.0%	0.0%
turn on the stove and put the moka pot on it	44	100.0%	98.0%	+2.0%
put the black bowl in the bottom drawer of the cabinet and close it	67	96.0%	94.0%	+2.0%
put the white mug on the left plate and put the yellow and white mug on the right plate	87	70.0%	100.0%	-30.0%
pick up the book and place it in the back compartment of the caddy	66	92.0%	100.0%	-8.0%
put the white mug on the plate and put the chocolate pudding to the right of the plate	86	80.0%	98.0%	-18.0%
put both the alphabet soup and the cream cheese box in the basket	65	98.0%	98.0%	0.0%
put both moka pots on the stove	31	92.0%	80.0%	+12.0%
put the yellow and white mug in the microwave and close it	58	94.0%	92.0%	+2.0%

1053
1054
1055
1056
1057
1058
1059
1060
1061
1062
1063
1064
1065

Table 14: Complete hyperparameter configuration used in all main experiments.

QK-related Param	Value	Dynamic Param	Value	Viz/Eval Param	Value
qk_keep_enabled	true	use_dynamic_visual_strategy	true	num_trials_per_task	50
qk_layer	0	decision_method	adjacent	overlay_pruned_color	[0,0.255]
qk_keep_ratio	0.5	adjacent_variant	extrema	overlay_pruned_alpha	120
qk_keep_split	[0.4, 0.6]	adjacent_extrema_window	3	video_fps	10
random_keep_ratio	0.5	adjacent_lookback	2		
random_state_prob	0.5	delta_method	net		
random_seed	42	limit_consecutive_pruned_enabled	true		
		limit_max_consecutive_pruned	3		

1074
1075
1076
1077
1078
1079